Bottom-up Fabrication of Semiconductive Metal-Organic Frameworks Ultrathin Films

Víctor Rubio-Giménez,[†[a]] Marta Galbiati,[† [a]] Javier Castells-Gil,[[a]] Neyvis Almora-Barrios, [[a]] José Navarro-Sánchez,[[a]] Garin Escorcia-Ariza,[[a]] Michele Mattera,[[a]] Thomas Arnold,[[b]] Jonathan Rawle,[[b]] Sergio Tatay*[[a]], Eugenio Coronado[[a]] and Carlos Martí-Gastaldo*[[a]]

[a] Instituto de Ciencia Molecular, Universitat de València, Catedrático José Beltrán 2, 46980 Paterna, Spain
[b] Diamond Light Source, Harwell Science and Innovation Campus, Chilton, Didcot OX11 0DE, UK.

Dedication ((optional))

Abstract: Though generally considered insulating, recent progress on the discovery of conductive porous Metal-Organic Frameworks (MOFs) offers new opportunities for their integration as electroactive components in electronic devices. Compared to classical semiconductors, these metal-organic hybrids combine the crystallinity of inorganic materials with easier chemical functionalization and processability. Still, future development depends on our ability to produce high-quality films with fine control over their orientation, crystallinity, homogeneity and thickness. Here we make use of Self-Assembled Monolayer (SAM) substrate modification and bottom-up techniques to produce highly-oriented, ultrathin, conductive films of Cu-CAT-1. Our approach permits to fabricate and study the electrical response of MOF-based devices incorporating the thinnest MOF film reported thus far (10 nm thick).

Research involving electrically conductive porous Metal-Organic Frameworks (MOFs) is just starting to blossom, with very interesting examples of highly conductive bulk materials.[1] Compared to classical semiconductors, MOFs combine the three-dimensional order and high crystallinity of inorganic solids with the synthetic versatility (fine manipulation of optical/electrical properties) and processability of organic materials. These porous solids also offer the possibility of indirectly manipulating their properties, and even introduce non-native functionalities, by loading of active guests.[2] The integration of porous, conductive MOFs as active semiconductor channels might offer new perspectives for the development of electronic devices relevant to fields of key environmental value like photovoltaics, photo-catalysis or sensing.[3-5] However, this possibility remains at a very early stage with only a few reports on the semiconducting behaviour of MOFs. Even more, there are important issues related to the fabrication of thin films that need to be addressed prior to device development. [6] Electronic and optoelectronic applications require the fabrication of high-quality films with exquisite control over their thickness, morphology, density, crystallinity, roughness and orientation. These are all severe requirements for device performance. To date, most of reports that meet these criteria involve somewhat thick films (> 100 nm)[7-9] or flakes with micrometric lateral dimensions[10] prepared by direct solvothermal reaction or interphase deposition onto bare substrates.

We have recently demonstrated that the combination of bottom-up techniques, such as the functionalization of substrates with self-assembled monolayers (SAM) coupled to Langmuir-Blodgett (LB) transfer and Layer-by-Layer (LbL) sequential deposition, enables the production of homogeneous electronically active ultrathin MOF films across millimetre-scale areas with fine control over the desired thickness.[11-13] Compared to other methodologies like the epitaxial growth of SURMOFs,[14] this approach is better fitted to process layered MOFs that do not require the presence of pillaring linkers to mediate soft coordination bonds between neighbouring layers and have pore channels normal to the substrate plane.[15] In this case, MOF structure is replicated by sequential transfer of the constituting 2D layers, which have been previously assembled at the air-liquid interphase.[16] This avoids direct nucleation of the metal planes on the substrate to prevent the formation of multiple inter-grain boundaries that would increase surface roughness and thus electrical resistance, and endows control over the thickness of the film. This strategy benefits from the use of SAMs to assist the transfer of the layers, thereby enlarging the landscape of substrates at choice.

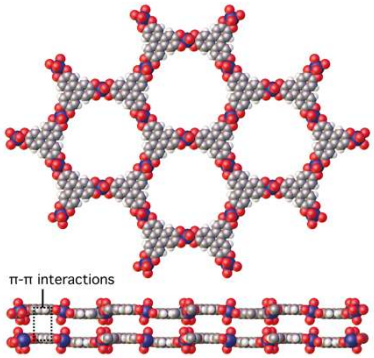

Figure 1. Scheme of the structure of 2D metal chatecolates (M-CAT-1).

Though we originally demonstrated the value of this approach by using NAFS-1 as a model system,[12,17] this 2D MOF is not adequate to develop semiconducting, porous interfaces as it only displays moderate conductivity and lacks accessible

[a] V. Rubio-Giménez, Dr. M. Galbiati, J. Castells-Gil, N. Almora-Barrios, J. Navarro-Sánchez, G. Escorcia-Ariza, M. Mattera, Dr. S. Tatay, Prof. E. Coronado, Dr. C. Martí Gastaldo
Instituto de Ciencia Molecular
Universitat de València
Catedrático José Beltrán 2, 46980 Paterna (Spain)
e-mail: carlos.marti@uv.es, sergio.tatay@uv.es
Homepage: http://www.icmol.es/funimat

[b] Dr. T. Arnold, Dr. J. Rawle
Diamond Light Source
Harwell Science and Innovation Campus
Chilton, Didcot OX11 0DE (United Kingdom)

[†] V.R.-G. and M. G. contributed equally to this work.

Supporting information for this article is given via a link at the end of the document.

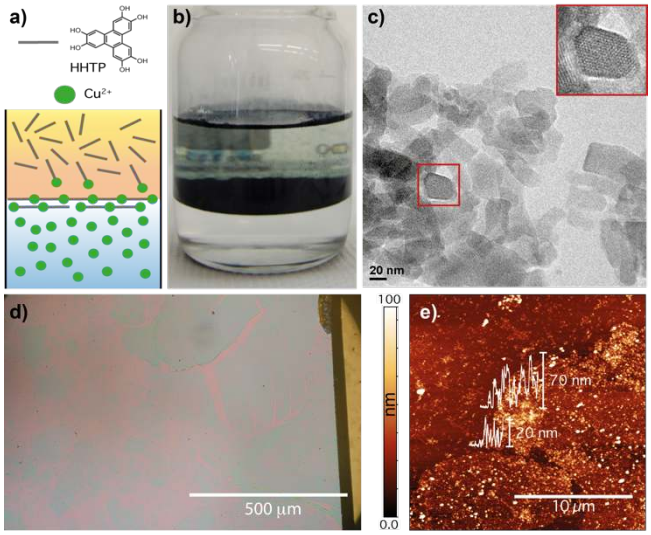

Figure 2. a) Scheme for the formation of LL interfacial films of Cu-CAT-1. b) Photograph of the film formed after dispersing an organic solution of HHTP on top of an aqueous solution of Cu(II) ions. c) HR-TEM image of the nanometric sheets in the film. Inset shows a zoom-in image revealing the hexagonal pattern of an individual 40 nm nanosheets. d) Optical and e) AFM topographic image of the film transferred to Si/SiO_2 substrates. Profiles superimposed show the typical variety of thicknesses of the blocks of nanosheets transferred to SAM modified substrate.

porosity. Here, we extend our strategy to the fabrication of ultrathin films (≤ 50 nm) of an electrically conductive porous metal catecholate MOF (Cu-CAT-1), better suited for this purpose. We report two complementary deposition strategies, a facile and versatile liquid-liquid (LL) procedure and a highly controlled LB and LbL hybrid approach. In both cases, pre-functionalization of substrates with hydrophobic SAMs serves to substantially improve substrate transfer to enable fabrication of FET-type devices.

M-CAT-1 (M(II) = Ni, Co and Cu) were originally reported by Yaghi and collaborators as bulk solids, prepared by solvothermal synthesis.[18] Coordination of metal centers with 2,3,6,7,10,11-hexahydroxytriphenylene (HHTP), a conjugated polyaromatic tricatecholate ligand, results in extended 2D graphene-like honeycomb grids that conform a porous, layered structure as result of π-π stacking (**Figure 1**). Just like other 2D π-conjugated systems based on amino and thiol phenylene/benzene linkers,[9,19,20] the M-CAT-1 family displays high conductivity thanks to strong charge delocalization across the plane due to the good energetic overlap between the metal nodes and the organic linker in its oxidized form. The combination of in-plane conductivity and layered structure makes these systems ideal candidates to produce ultrathin films by controlled transfer of pre-formed layers, that preserve the electronic properties of the bulk. Our approach relies on the formation of 2D MOF nanosheets that can be then sequentially deposited onto surfaces as ultrathin films. As shown in **Figure 2a**, this possibility was first evaluated by a LL room temperature interphase reaction that occurs when an ethyl acetate HHTP organic solution is carefully spread onto a $Cu(OAc)_2$ water solution. After a few minutes, a bluish film starts to form at the interphase, which becomes thicker and darker in colour with time (**Figure 2b**). This solid shows an identical PXRD pattern to that reported for Cu-CAT-1 prepared by solvothermal methods (**Figure SI1**).[18] Additionally, we manually transferred part of the interfacial film to a microscopy grid to analyse its internal structure by high-resolution transmission electron microscopy (HRTEM), which reveals that it is composed of multiple nanosheets with rounded edges and lateral sizes ranging from 20 up to 200 nm (**Figure 2c, SI2**). High magnification permits identifying a hexagonal arrangement of channels consistent with the honeycomb-like layers of M-CAT-1 MOFs. Unfortunately, these nanosheets are very sensitive to beam irradiation and these features are rapidly lost under prolonged exposition times. Although selected area electron diffraction (SAED) typical of a polycrystalline material was briefly visible, it quickly disappeared in the order of a second, preventing the acquisition of static images. According to HRTEM-EDX (EDX, energy-dispersive X-ray analysis), nanosheets display a homogeneous distribution of copper, carbon and oxygen with no presence of other elements (**Figure SI2**). Next, we transferred as-made films onto 3 x 3 cm SiO_2 substrates pre-functionalized with octadecyltrichlorosilane (OTS). This results in an unbalanced transfer of micrometric-sized nanosheet blocks, which under the optical microscope appear noticeably cracked and have sharp straight edges (**Figure 2d**). The empty space in-between the bigger blocks are sometimes covered with thinner ones. Atomic force microscopy (AFM) and scanning electron microscopy (SEM) images confirm partial cracks in the films with heterogeneous thickness ranging from 10 to 70 nm (**Figure 2e and SI3**).

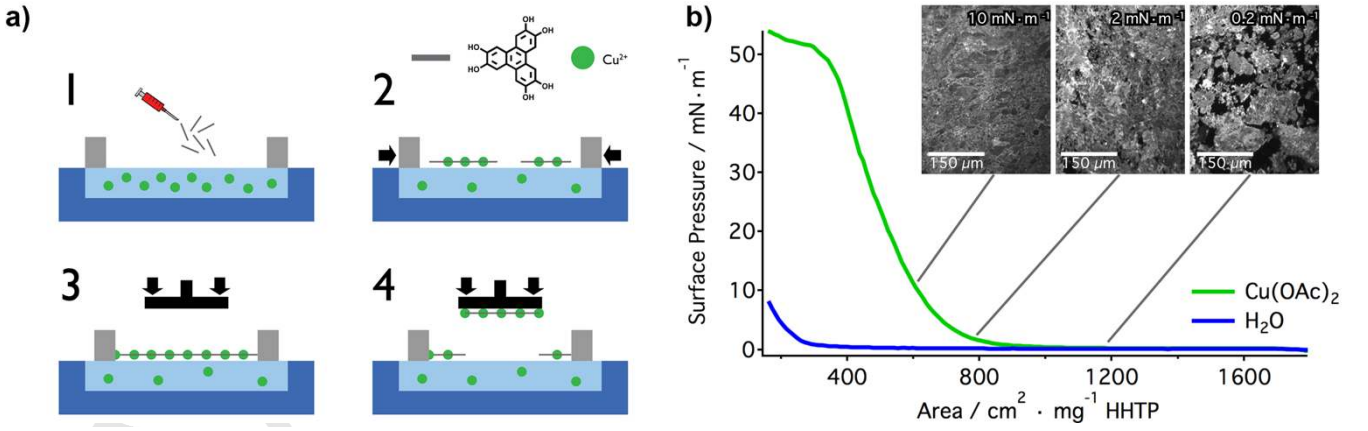

Figure 3. a) Fabrication of homogeneous Cu-CAT-1 films with controllable thickness by sequential transfer of nanosheets: formation (1), compression (2), optimal pressure for continuous layer (3) and transfer to the substrate (4). b) BAM images taken at different points of the pressure-area isotherm. The area for which the surface pressure starts to rise is clearly larger for the $Cu(OAc)_2$ subphase than for the pure water subphase. This is indicative of the formation of Cu-CAT-1 nanosheets.

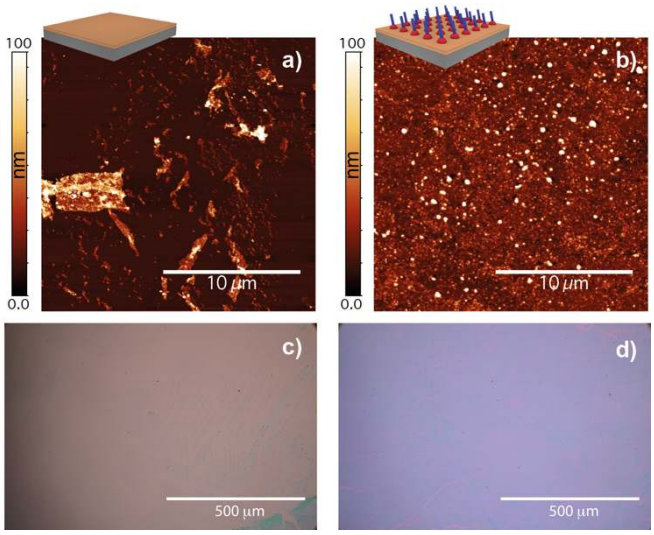

Figure 4. Topographic AFM and optical microscopy images of 1 transfer onto bare Si/SiO_2 (a & c) and onto Si/SiO_2 previously functionalized with OTS (b & d), confirming the key role of SAM functionalization for producing homogeneous films.

Whereas this strategy has been recently used for fabricating thicker films of 2D π-conjugated coordination polymers (ca. 100-350 nm),[7,21,22] our results suggest that it is not suitable to produce Cu-CAT-1 homogeneous ultrathin films below 50 nm as it lacks real control over the homogeneity of interfacial film. Based on our previous work with NAFS-1,[12] we chose to use a more sophisticated alternative to enable the formation of more homogeneous films with reproducible thickness and a precise control of the transfer process. As seen in **Figure 3a**, this involves compression of the floating nanosheets of Cu-CAT-1 formed at the air-liquid interphase of a LB trough by bringing together the moveable barriers until forming a continuous floating film. Next, the compressed film is transferred to a substrate via the Langmuir-Schaefer (LS) method. The formation and compression of the MOF nanosheets was explored using Brewster angle microscopy (BAM; **Figure 3b**). Initially, at low surface pressure, dispersed blocks of nanosheets appear moving randomly at high speeds. These can be brought together into a continuous film with barrier compression, thus when surface pressure starts to rise (0.2 $mN \cdot m^{-1}$) these blocks start grouping together until empty spots are no longer visible (10 $mN \cdot m^{-1}$). Finally, at high surface pressures the floating film collapses due to excessive pressure (above 50 $mN \cdot m^{-1}$). The area at which surface pressure starts to rise is considerably lower than expected for a single layer of HHTP molecules lying flat on the water subphase surface. Given that synchrotron surface XRD points to the HHTP in the nanosheets adopting a parallel orientation with the substrate (see infra), we attribute this low area to two main causes: (i) partial solubility of HHTP in water and (ii) the formation of multi-layered nanosheets due to the strong π-π interactions in-between aromatic cores of HHTP molecules. The transfer to a solid support of the floating films grown at optimal pressure was done with the LS method, by slowly approaching a face-down substrate to the water surface until contact, the substrate is then quickly lifted. After the transfer, films were rinsed with water and methanol to get rid of any unreacted precursors and then dried by blowing N_2. Additionally, we manually transferred the floating film to a microscopy grid to analyse it by HRTEM (**Figure SI4**), which reveals similar but smaller and thinner nanosheets than for LL. Therefore, these nanosheets are even more sensitive to beam irradiation and thus it was not possible to obtain images neither of their internal honeycomb-like structure nor SAED as both disappeared in fractions of a second. HRTEM-EDX reveals a homogeneous distribution of copper, carbon and oxygen without any other elements.

Our experiments suggest that surface wettability is vital to yield homogeneous films. Transfer to clean hydrophilic substrates (CA < 20º) such as silicon, ITO and Au, yields inhomogeneous coatings with films covering only isolated areas of the substrate (**Figure SI5**). However, as for LL, if those same substrates are previously functionalized with the appropriate alkyl SAM, LB transfer is favoured to produce high-quality films featuring complete coverage over large areas (millimetric areas after one transfer; **Figure 4**). We used OTS for SiO_2, 1-dodecylphosphonic acid (C12P) for ITO and 1-dodecanethiol (C12S) for Au, turning the surface hydrophobic in all cases (CA >100º). Further SEM (**Figure SI6**) and AFM (**Figure SI7**) analysis confirmed the improved quality of the LB film compare to LL films, showing a much more homogeneous coverage. As

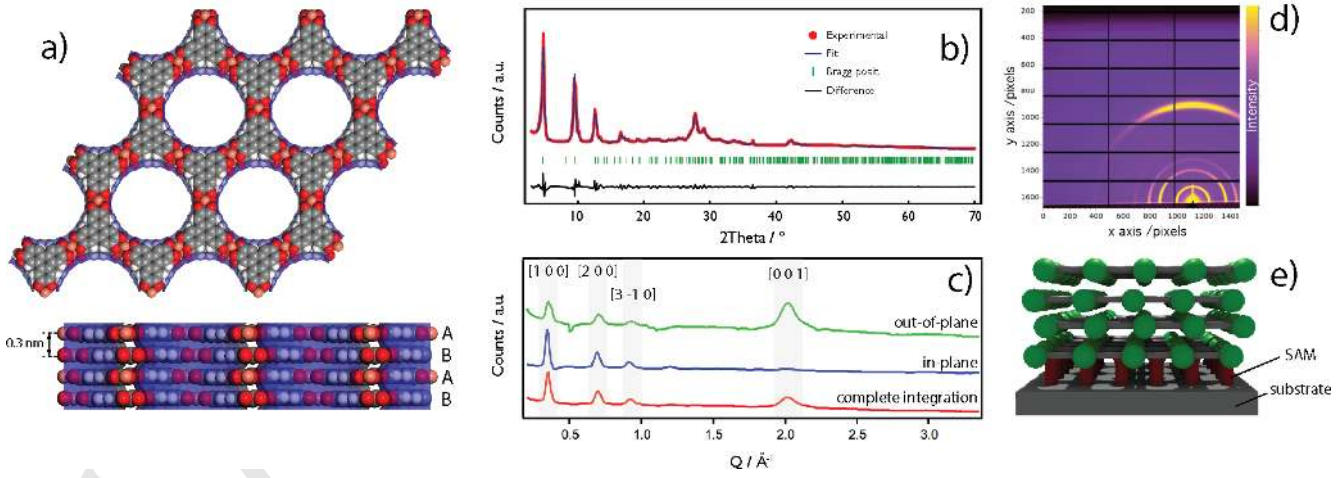

Figure 5. a) Proposed layered structure of Cu-CAT-1 from slipped-parallel AB stacking of hexagonal layers. b) Lebail refinement of the PXRD pattern of the bulk solid. c) Complete, in-plane and out-of-plane 2D-GIXRD profiles of LL films transferred to Si/SiO_2-OTS. Grey panels highlight most intense diffraction lines. Changes in intensity account for the highly-oriented nature of the film. d) 2D-GIXRD image from which the profiles were extracted. e) Scheme depicting the formation of oriented films by SAM-directed transfer.

shown in figure SI8, on OTS-functionalized Si/SiO_2 after one transfer we obtained and average root-mean square (RMS) roughness of 7.8 ± 0.7 nm over 1 μm^2 areas, indicative of small corrugations in the top surface and a thickness of 10.1 ± 1.1 nm from scratching experiments. By assuming the layered structural model proposed below for Cu-CAT-1, this would correspond roughly to the transfer of 30 monolayers based on an interlayer separation of 0.3 nm. As preliminarily suggested by the BAM study, this is consistent with strong π-π interactions between neighbouring layers likely to favour their stacking preventing the formation and transfer of monolayers. This process can be sequentially repeated for controllable thickness, AFM scratch experiments reveal an increase of 10.2 ± 0.6 nm per transfer cycle. This was confirmed with UV-vis spectroscopy by using transparent C12P-functionalized ITO substrates. Each transfer deposits the same amount of material for a linear increase of the thickness and absorption maximum with the number of transfers. The concomitant increase of the 356 and 622 nm bands associated to aromatic π-π* and ligand-to-metal charge transfer transitions, rules out simple transfer of the linker (**Figure SI9**). Infrared reflectance absorption spectroscopy (IRRAS) onto C12S-functionalized Au substrates also sustains metal complexation indicative of the formation of the MOF as confirmed by the presence of equivalent vibrational modes in the Cu-CAT-1 prepared solvothermally and the film (**Figure SI10**). High-resolution X-ray photoelectron (XPS) survey spectrum confirms the presence of the constitutive elements of Cu-CAT-1 (C, O, and Cu; **Figure SI11**). The Cu 2p region of the LL and LB films spectra (**Figure SI12**) shows a main Cu($2p_{3/2}$) component at 935 eV, accompanied by less intense shakeup satellite peaks at higher binding energies that denote to the presence of Cu(II) species in the films comparable to that of Cu-CAT-1 prepared by solvothermal synthesis, and ruling out changes in copper oxidation state upon reaction with HTTP, in consonance with the Cu LMM Auger spectra (**Figure SI13**). The overall amount of Cu and O species in the solvothermal solid and the films was quantified from integration of their peak areas (Cu $2p_{3/2}$ and O 1s). The average Cu:O ratio is slightly superior to the theoretical 1:4 value for all cases. This excess of O is likely due to the presence of solvent molecules in the pores.

Though structurally similar to its Co- and Ni-CAT-1 counterparts, the structure of the Cu(II) phase remained still unknown. We lacked of a reliable model that permitted confirming the formation of oriented, crystalline films upon transfer. Hence, by using the reported structure of $Ni_3(HITP)_2$ as starting model,[9] we used density functional theory calculations and the Reflex module in Materials Studio to generate and optimize simulated structures that guided the refinement of the PXRD of Cu-CAT-1 prepared by solvothermal synthesis (see Figure SI14 and SI15 for full details). PXRD was indexed to a hexagonal unit cell with dimensions a = 21.3641 Å and c = 6.7295 Å. As shown in **Figure 5b**, LeBail refinement converged with excellent residual values (Rwp = 3.26%, Rp= 2.31%). Cu-CAT-1 displays a layered structure built up from the stacking of 2D honeycomb grids assembled from the coordination of metal centers with the HHTP linker. Compared to Co- and Ni-CAT-1, that results from the packing of two types of layers, Cu-CAT-1 is built only from the packing of 2D extended layers of square planar Cu(II) units coordinated to semiquinone tricatecholate units following a slipped-parallel (AB) packing mode. This results in the formation of 1D hexagonal channels with internal diameters close to 1.6 nm. Just like with $Ni_3(HITP)_2$, this packing mode is energetically more favourable than the eclipsed configuration according to our DFT calculations (Figure SI15). The structure and orientation of LL thin films (2 transfers) deposited onto SiO_2-OTS were investigated by synchrotron Two-dimensional grazing incidence X-ray diffraction (2D-GIXRD, λ = 0.8 Å, room temperature), for which a diffraction pattern was collected in a single shot image (**Figure 5d**). Then, complete, in-plane and out-of-plane profiles were extracted by simple sector integration of the Q-space image (see **Figure SI16**). As seen in **Figure 5b**, the complete 2D-GIXRD pattern matches with the PXRD of Cu-CAT-1 prepared solvothermally confirming the crystallinity of the film.[18] Moreover, the drastic change in intensity of the (001) peak in the in-plane and out-of-plane XRD profiles proves the formation of highly-oriented films that preferably lie with the ab plane parallel to the substrate surface. Synchrotron 2D-GIXRD was also measured for LB ultrathin films onto SiO_2-OTS (2 transfers, 20 nm), showing an equivalent change in the intensity of the (001) peak (**Figure SI17**). The porosity of Cu-CAT-1 was studied by N_2 adsorption-desorption measurements at 77 K. For comparison, we studied the bulk material prepared via solvothermal reaction and the nanosheets prepared by biphasic LL synthesis at room temperature. As described above, this produces similar nanosheets than the LB method but can be scaled up for sample availability. Both materials show a reversible type-I N_2 uptake with no hysteresis (**Figure SI18**), which confirms microporosity Calculated multi-point BET surface areas for solvothermal and room temperature synthesized Cu-CAT-1 of 348 and 334 $m^2 \cdot g^{-1}$ confirm that porosity remains accessible for the LL film. BET values remain

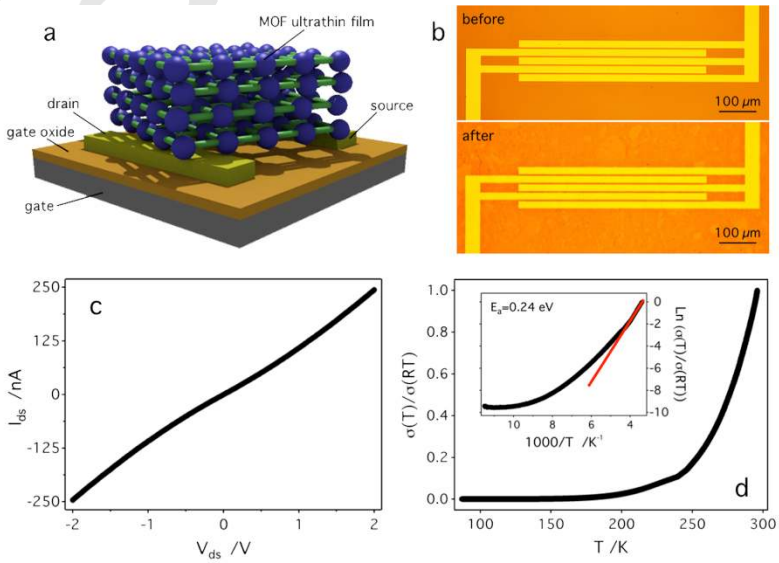

Figure 6. a) Schematic of a Cu-CAT-1 bottom-gate bottom-contact MOF-based device. b) Optical microscope picture of a real device with interdigitated pre-patterned Au electrodes before/after LB transfer of a 10 nm thick film. c) Room temperature I-V curve for the device (2.5 μm channel length). Measurement was performed in vacuum. d) Electrical conductivity (σ) of the device as a function of temperature measured at a bias voltage of V_{ds}=1 V and normalized by the electrical conductivity measured at room temperature (σ(RT)). The inset shows the plot of Ln(σ(T)/ σ(RT)) versus 1/T. From the linear fit at high temperature (red line) we estimate an activation energy of 0.24 eV.

close to those reported for the Ni and Co-CAT-1, confirming the structural similarities between both phases.

The ability to produce high-quality, well-oriented ultrathin films regardless the substrate is perfectly fitted to investigate the electrical properties of nanometric thick Cu-CAT-1 in MOF-based devices (**Figure 6a**). By following the protocol described above, we fabricated bottom-contact configuration devices by sequential transfer of Cu-CAT-1 films on 500 µm width interdigitated Au electrodes pre-patterned on top of a Si/SiO_2 substrate (SiO_2 230 nm thick and highly doped n-type Si acting as dielectric and gate, respectively, to eventually apply a bottom-gate voltage) and channel lengths ranging between 2.5 µm and 20 µm. Before film deposition, we functionalized Au and SiO_2 with C12S and OTS to assist the MOF transfer onto the electrodes and dielectric, respectively. We chose to use bottom contact pre-patterned electrodes to avoid potential contamination or damage to the MOF film during the electrode fabrication process. LB thin films from 50 nm down to 10 nm thick were prepared by the sequential transfer of Cu-CAT-1 via the Langmuir-Schaefer (LS) method. The complete coverage of the device after the thin MOF film transfer was confirmed using optical microscopy as shown in **Figure 6b**.

Figure 6c shows a typical I-V curve of a device with a MOF film thickness of 10 nm and a channel length of 2.5 µm, measured in vacuum. I-V curves show a linear response that denotes ohmic contacts between the Au electrodes and Cu-CAT-1. Measurements were well reproducible between different samples and between devices fabricated over the same substrate but laying some millimetres away from each other. This confirms the good homogeneity and reproducibility of our transferred Cu-CAT-1 films. Room temperature conductivity (σ_{RT}) of the films measured in vacuum was calculated to be in the order of 10^{-4} $S \cdot cm^{-1}$. As expected, this is below the conductivity of 2 x 10^{-1} $S \cdot cm^{-1}$ reported for Cu-CAT-1 single crystals,[18] due to intrinsic differences in the nature of the samples studied (crystals vs polycrystalline thin film). However, reported conductivity is still comparable to those of typical organic conductors (>10^{-6} $S \cdot cm^{-1}$).[17] **Figure 6d** shows dependence of the electrical conductivity as function of the temperature normalized to the electrical conductivity at room temperature (σ_{RT}). Conductivity follows an exponential decrease upon cooling, thus confirming the semiconducting nature of Cu-CAT-1. We observe a non-linear relation between ln(σ (T)/ σ (RT)) and the reciprocal of the device temperature (inset Figure 6d) as reported for substantially thicker MOF films[10,21] and commonly observed for conducting coordination polymers.[23] No single conduction law can fit the entire curve of the conductivity. Figure 6 suggests that there are at least two types of conduction mechanisms contributing to the conductivity in different temperature ranges. For the high temperature range (T > 240 K), we have succeeded to fit the conductivity data to an Arrhenius law. This suggests that a simple thermal activation process dominates the electrical conduction in the film. From the linear fit at high temperature we estimate a fundamental band gap ($E_g = 2E_a$) of about 0.48 eV.[1] A further decrease in temperature (T < 240 K) leads to a deviation from the linearity, indicating a change in conduction mechanism, which may be due to the dominance of variable range hopping conduction. In Mott's 3D variable range hopping, the conductivity for three-dimensional (3D) systems is expected to follow a $T^{-1/4}$ dependence. Over the temperature region 200–125 K ln(σ (T)/ σ (RT)) Cu-CAT-1 data is well fitted to the 3D variable range hopping model (**Figure SI19**),[22] suggesting that inter- and intra-layer charge transport operates across and between MOF 2D layers. This is consistent with the existence of π - π interactions between Cu-CAT-1 layers, in accordance with XRD data.

We also analysed the effect of film thickness and channel length alongside the fabrication method over the electrical response of our devices. We observe an exponential decrease of device resistance with increasing thickness from 10 nm to 50 nm (**Figure SI20**). On the contrary, as shown in **Figure SI21**, the resistance increases exponentially upon increasing the channel length between 2.5 µm and 20 µm. It is worth noticing the low statistical dispersion of all these measurements, which further confirms the excellent quality of the Cu-CAT-1 films and the reproducibility of the transfer process. We next compared the electrical response of devices fabricated by using LL and LB techniques for identical film thickness between 1 and 5 transfers (≈10 nm to 50 nm). This information might be relevant to the use of MOFs as electroactive, porous interfaces in electronic devices. This study confirms that, when compared to the LB ones, LL series show higher and more disperse resistance values and a less clear dependence of the resistance with increasing thickness (**Figure SI22a**). We ascribe this effect to the poorer homogeneity of the LL films and the worse reproducibility of the transfer method, for a higher number of grain boundaries that can result in worse electrode/film interfaces. These results highlight the importance of the fabrication method over the electrical response of the device and confirm SAM-assisted LB as a suitable and very reliable method for the fabrication of high-quality conductive ultrathin MOF films on arbitrary substrates.

We next investigated the electrical response of the devices when a back-gate voltage is applied to show their possible application in FETs. As reported in **Figure SI23**, as-transferred films show small modulation of source-drain current with back gate voltage. The channel current gradually increases with decreasing V_g, which indicates a p-type transport in Cu-CAT-1 (**Figures SI23b and SI23c**). The small modulation we observe might be attributed to a bad contact between the MOF thin film and the OTS/SiO_2 layer to avoid this problem further optimization will be needed for these devices. For example, top-gate configurations will be probably more suitable to be explored in the future. Finally, we investigated the impact of atmosphere over the electrical properties of the films with equivalent measurements at ambient pressure and in vacuum. As shown in **Figure SI24**, we observe a systematic decrease of about one order of magnitude in the resistance of the devices when they are measured in vacuum, regardless the film thickness. Previous reports confirm the effect of environmental conditions over MOF electrical response.[24] Conductivity of Cu-CAT-1 films might be affected by guest uptake or structural changes affecting the coordination geometry of Cu(II) centers for modification of the electronic structure of the solids. We are currently investigating the interplay between different external stimuli and conductivity changes to provide further insights on this phenomenon.

MOF-based electronics might become a striking reality with immense potential for future technological development. Still, further advancement depends on our ability to produce high-quality films onto a wide variety of substrates with control over their orientation, crystallinity, homogeneity and thickness. We report two routes based on the assembly of free floating (LL) or compressed (LB) 2D MOF nanosheets for the fabrication of

ultrathin films (≤ 50 nm) of electrically conductive Cu-CAT-1 that fulfil these requirements. Efficient transfer relies on the modification of the substrate with a SAM, conferring versatility to our method that might be extended to different substrates depending on the targeted application. We demonstrate the value of our approach to fabricate MOF-based devices and study the electrical conductivity on the thinnest films (10 nm thick) reported thus far. Direct comparison between two families of devices is used to provide information on the effect of the fabrication method, film thickness and channel length over their electrical response, which might be of fundamental value for the integration of MOFs in electronic devices. Just like the development of silicon-based electronics, the fabrication of MOF-based devices will also benefit from close collaboration between synthetic chemists, materials scientists and physicists. We expect mutual interaction will help evolving from the synthetic aspects of MOF chemistry, far better understood now, into the development of functional devices that exploit all their potential.

Experimental Section

LB film preparation. First, a KSV Nima PTFE-coated Langmuir minitrough (8720 mm^2) was thoroughly cleaned with methanol and dichloromethane using surfactant-free wipes and the it was filled with 0.5 mM $Cu(OAc)_2 \cdot H_2O$ aqueous solution as a subphase. Next, the surface of the subphase was carefully cleaned by mild surface-touch vacuuming. Next, 150 µL of a freshly prepared solution of HHTP (1 mM nominal concentration) in chloroform/methanol (3:1, v/v) were carefully spread drop-by-drop onto the subphase using a Hamilton microsyringe. Surface pressure (π) was monitored using a paper Wilhelmy plate under a continuous pressing speed for two barriers of 10 $mm \cdot min^{-1}$. Sequential transfers were performed using the LS method (horizontal dipping) at a surface pressure of 10 $mN \cdot m^{-1}$. The substrate was slowly approached to the surface at a speed of 0.5 $mm \cdot min^{-1}$ and raised at a speed of 10 $mm \cdot min^{-1}$. Then it was submerged in water and methanol for 1 min each and dried by blowing N_2. Experiments were performed in a class 10000 clean room at 22ºC and 50% humidity.

Liquid-liquid (LL) synthesis. A 1 mM solution of HTTP (nominal concentration) in ethyl acetate was carefully layered onto a 1.5 mM $Cu(OAc)_2 \cdot H_2O$ aqueous solution. The resulting biphasic mixture was left undisturbed for 24 hours. After removing the organic layer, the interphasial film was either transferred to a substrate by horizontal dipping or the aqueous phase was centrifuged to isolate a dark blue powder.

Solvothermal synthesis. Bulk Cu-CAT-1 was prepared following a literature procedure.[18]

Acknowledgements

This work was supported by the EU (ERC Stg Chem-fs-MOF), Spanish MINECO (Unit of Excellence María de Maeztu MDM-2015-0538), and the Generalitat Valenciana (GV/2016/137).. V.R.-G. thanks the Spanish MECD for a FPU predoctoral grant; M.G. thanks the European Union Horizon 2020 Marie Curie Actions under the project SPIN2D (H2020/2014-659378); G.E-A. thanks the Generalitat Valenciana for a Santiago Grisolía predoctoral grant. C.M.-G. and J.C-G. thank the Spanish MINECO for a Ramón y Cajal Fellowship and a FPI predoctoral grant respectively. We are also grateful to Ángel Lopéz-Muñoz, Eva Tormos and Francisco González González for their technical support, and Dr. Jacob Filik for his assistance analysing synchrotron XRD data. Prof. Núria López and Tirant-RES are acknowledged for the computational resources.

Keywords: Metal-Organic Framework • ultrathin film • electrical conductivity • self-assembled monolayer • device

[1] L. Sun, M. G. Campbell, M. Dincă, *Angew. Chem. Int. Ed.* **2016**, *55*, 3566–3579.
[2] A. A. Talin, A. Centrone, A. C. Ford, M. E. Foster, V. Stavila, P. Haney, R. A. Kinney, V. Szalai, F. El Gabaly, H. P. Yoon, et al., *Science* **2014**, *343*, 66–69.
[3] I. Stassen, N. Burtch, A. Talin, P. Falcaro, M. Allendorf, R. Ameloot, *Chem. Soc. Rev.* **2017**, *46*, 3185–3241.
[4] M. Usman, S. Mendiratta, K. L. Lu, *Adv. Mater.* **2017**, *29*, 1605071–1605075.
[5] M. D. Allendorf, A. Schwartzberg, V. Stavila, A. A. Talin, *Chem-Eur J.* **2011**, *17*, 11372–11388.
[6] J. Liu, C. Wöll, *Chem. Soc. Rev.* **2017**, *46*, 5730–5770.
[7] G. Wu, J. Huang, Y. Zang, J. He, G. Xu, *J. Am. Chem. Soc.* **2017**, *139*, 1360–1363.
[8] M. G. Campbell, D. Sheberla, S. F. Liu, T. M. Swager, M. Dincă, *Angew. Chem. Int. Ed.* **2015**, *54*, 4349–4352.
[9] D. Sheberla, L. Sun, M. A. Blood-Forsythe, S. Er, C. R. Wade, C. K. Brozek, A. Aspuru-Guzik, M. Dinča, *J. Am. Chem. Soc.* **2014**, *136*, 8859–8862.
[10] N. Lahiri, N. Lotfizadeh, R. Tsuchikawa, V. V. Deshpande, J. Louie, *J. Am. Chem. Soc.* **2017**, *139*, 19–22.
[11] R. Dong, M. Pfeffermann, H. Liang, Z. Zheng, X. Zhu, J. Zhang, X. Feng, *Angew. Chem. Int. Ed. Engl.* **2015**, *54*, 12058–12063.
[12] V. Rubio-Giménez, S. Tatay, F. Volatron, F. J. Martínez-Casado, C. Martí-Gastaldo, E. Coronado, *J. Am. Chem. Soc.* **2016**, *138*, 2576–2584.
[13] Y. Jiang, G. H. Ryu, S. H. Joo, X. Chen, S. H. Lee, X. Chen, M. Huang, X. Wu, D. Luo, Y. Huang, et al., *ACS Appl. Mater. Interfaces* **2017**, *9*, 28107–28116.
[14] O. Shekhah, J. Liu, R. A. Fischer, C. Wöll, *Chem. Soc. Rev.* **2011**, *40*, 1081–1106.
[15] J. Liu, B. Lukose, O. Shekhah, H. K. Arslan, P. Weidler, H. Gliemann, S. Bräse, S. Grosjean, A. Godt, X. Feng, et al., *Sci. Rep.* **2012**, *2*, 921–925.
[16] R. Sakamoto, K. Hoshiko, Q. Liu, T. Yagi, T. Nagayama, S. Kusaka, M. Tsuchiya, Y. Kitagawa, W.-Y. Wong, H. Nishihara, *Nat. Commun.* **2015**, *6*, 6713.
[17] R. Makiura, S. Motoyama, Y. Umemura, H. Yamanaka, O. Sakata, H. Kitagawa, *Nat. Mater.* **2010**, *9*, 565–571.
[18] M. Hmadeh, Z. Lu, Z. Liu, F. Gándara, H. Furukawa, S. Wan, V. Augustyn, R. Chang, L. Liao, F. Zhou, et al., *Chem. Mater.* **2012**, *24*, 3511–3513.
[19] T. Kambe, R. Sakamoto, T. Kusamoto, T. Pal, N. Fukui, K. Hoshiko, T. Shimojima, Z. Wang, T. Hirahara, K. Ishizaka, et al., *J. Am. Chem. Soc.* **2014**, *136*, 14357–14360.
[20] J. Cui, Z. Xu, *Chem. Commun.* **2014**, *50*, 3986–3988.
[21] X. Huang, P. Sheng, Z. Tu, F. Zhang, J. Wang, H. Geng, Y. Zou, C.-A. Di, Y. Yi, Y. Sun, et al., *Nat. Commun.* **2015**, *6*, 7408.
[22] A. J. Clough, J. W. Yoo, M. H. Mecklenburg, S. C. Marinescu, *J. Am. Chem. Soc.* **2015**, *137*, 118–121.
[23] G. Givaja, P. Amo-Ochoa, C. J. Gómez-García, F. Zamora, *Chem. Soc. Rev.* **2012**, *41*, 115–147.
[24] L. Sun, S. S. Park, D. Sheberla, M. Dincă, *J. Am. Chem. Soc.* **2016**, *138*, 14772–14782.

Entry for the Table of Contents (Please choose one layout)

COMMUNICATION

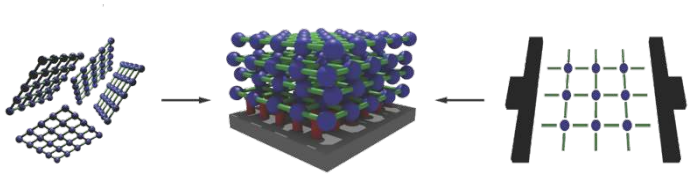

Ultrathin and conductive: by using SAM substrate modification and bottom-up techniques we produce highly-oriented, ultrathin, semiconductive films of the Metal-Organic Framework (MOF) Cu-CAT-1. Our approach enables fabrication and study of the electrical response of MOF-based devices incorporating the thinnest MOF film reported thus far (10 nm thick).

Víctor Rubio-Giménez, Marta Galbiati, Javier Castells-Gil, Neyvis Almora-Barrios, José Navarro-Sánchez, Garin Escorcia-Ariza, Michele Mattera, Thomas Arnold, Jonathan Rawle, Sergio Tatay, Eugenio Coronado and Carlos Martí-Gastaldo**

Page No. – Page No.

Title